

Primordial Gravitational Wave Probes of Non-Standard Thermal Histories

Annet Konings, Mariia Marinichenko,* Oleksii Mikulenko, and Subodh P. Patil

*Instituut-Lorentz for Theoretical Physics,
Leiden University, 2333 CA Leiden, The Netherlands*

(Dated: December 20, 2024)

Primordial gravitational waves propagate almost unimpeded from the moment they are generated to the present epoch. Nevertheless, they are subject to convolution with a non-trivial transfer function. Within the standard thermal history, shifts in the temperature-redshift relation combine with damping effects by free streaming neutrinos to non-trivially process different wavelengths during radiation domination, with subsequently negligible effects at later times. Presuming a nearly scale invariant primordial spectrum, one obtains a characteristic late time spectrum, deviations from which would indicate departures from the standard thermal history. Given the paucity of probes of the early universe physics before nucleosynthesis, it is useful to classify how deviations from the standard thermal history of the early universe can be constrained from observations of the late time stochastic background. The late time spectral density has a plateau at high frequencies that can in principle be significantly enhanced or suppressed relative to the standard thermal history depending on the equation of state of the epoch intervening reheating and the terminal phase of radiation domination, imprinting additional features from bursts of entropy production, and additional damping at intermediate scales via anisotropic stress production. In this paper, we survey phenomenologically motivated scenarios of early matter domination, kination, and late time decaying particles as representative non-standard thermal histories, elaborate on their late time stochastic background, and discuss constraints on different model scenarios.

I. PRELIMINARIES

Gravitational waves offer an almost uninterrupted view of the physics of the very early universe [1, 2]. Unlike electromagnetic probes, gravitational waves interact very weakly with matter. This makes them harder to detect but also limits the propensity for intervening matter along the line of sight (i.e. foregrounds) to obscure our view of their source. Although the scattering and absorption of gravitational waves during matter domination (MD) are feeble [3, 4], free streaming neutrinos have been shown to dissipate power via anisotropic stresses for sub-horizon modes of any stochastic background present during radiation domination (RD) [5]. Furthermore, changes in the temperature-redshift relation due to changing numbers of relativistic species, in addition to any entropy generating processes such as the quantum chromodynamics (QCD) crossover, conspire to process different wavelengths in a characteristic manner via a non-trivial transfer function [6, 7]. The result is a late time stochastic background with a power spectral density with various features that encode the particle content and thermal history of the early universe.¹

Any deviations from the thermal history of the universe will propagate through the transfer function, whether this be through modifications to the particle spectrum of the universe, or through the introduction of any additional entropy generating mechanisms (e.g. [20–27] for a partial survey), as well as possible bursts of anisotropic stress production. Given the limited number of probes that allow us to access the physics of the early universe before Big Bang nucleosynthesis (BBN), primordial gravitational waves appear to offer a constraining lever not accessible to other probes.

* Corresponding author: marinichenko@strw.leidenuniv.nl

¹ In principle, the transfer function would also have to account for lensing effects from the large scale structure foreground. We neglect this in what follows as we are primarily interested in scales for which this effect is negligible, although a more thorough treatment would certainly have to incorporate these effects [8–19].

In what follows, we explore the possibility of constraining non-standard thermal histories via observations of the late time stochastic background, taking for granted a nearly scale invariant spectrum of primordial gravitational waves. We do this by surveying a range of phenomenological models where the epoch between reheating and the terminal phase of radiation domination that onsets before nucleosynthesis may not correspond to pure radiation domination over its entirety. There are of course plausible scenarios in which the primordial spectrum departs from scale invariance. In what follows, we make the minimal assumption that this is not the case. Although any transfer function formalism is agnostic to the form of the input spectrum (provided it remains perturbatively small), one would not be able to cleanly distinguish spectral deviations induced by modified initial spectra from departures from the standard thermal history without additional observational input.

There are several ways in which one or more phase of non-radiation-like evolution could punctuate the epoch between reheating and nucleosynthesis. The field responsible for reheating (whether inflaton itself or some other intermediary) may undergo non-trivial dynamics around or before pre-reheating before it decays into Standard Model (SM) particles which then go on to thermalize. There could be additional light fields, such as axions which are frozen up until the Hubble scale drops below their mass, at which point they undergo coherent oscillations with a time averaged equation of state of cold dark matter [28–30], which may themselves produce additional light mediators and radiation [31–33]. One could also envisage departures from an equation of state of $w = 1/3$ from (dark sector) phase transitions, or the decay of heavy long lived particles. Although what is presented in the study that follows represents only a partial survey, it is straightforward to intuit how the dynamics of any given model directly translate into the power spectral density for the stochastic background: In the absence of any other source of anisotropic stress other than neutrinos², deviations from an equation of state parameter $w = 1/3$ translate into a suppression or enhancement of the high frequency plateau of the spectral density. Suppression occurs when ω decreases, and enhancement occurs when it increases in the intervening epoch(s) [35], with deviations at earlier times imprinting at shorter comoving scales, or higher frequencies, upon which features are superposed in the usual manner from shifts in the temperature-redshift relation and any intervening bursts of entropy production. If there are mechanisms to generate bursts of anisotropic stress production, then additional damping at intermediate scales also becomes a possibility.

In the sections that follow, we consider specific models of early matter domination (EMD), long-lived feebly interacting particles, and intervening kination as illustrative examples in which the mechanisms detailed above feature. We subsequently discuss prospects for constraining non-standard thermal histories with future and planned observations before offering our concluding thoughts. We discuss various details about our numerical implementation as we encounter them, referring to previous literature for the various derivations upon which this investigation relies.

II. THE GRAVITATIONAL WAVE TRANSFER FUNCTION

In what follows, we work in terms of the transfer function $\mathcal{T}(\tau, k)$ which describes the non-trivial evolution of gravitational wave modes $h_{\mathbf{k}}(\tau)$:

$$h_{\mathbf{k}}(\tau) \equiv h_{\mathbf{k}}^{\text{prim}} \mathcal{T}(\tau, k), \quad (1)$$

where τ denotes the conformal time, $k = |\mathbf{k}|$ is the comoving wavenumber, and $h_{\mathbf{k}}^{\text{prim}}$ is the primordial gravitational wave (PGW) amplitude shortly after horizon crossing during inflation.

² Photons, for example, are also a source of anisotropic stress. However, they are energetically subdominant during radiation domination and can be safely neglected [6, 7, 34]. If the particle content were to include additional light, weakly interacting particles (interactions rapidly dissipate anisotropic stress [3]), one would have to factor in their damping effects as well. This can be the case in scenarios involving dark photon production, as we discuss further.

For a given comoving scale k , the equation for transfer function $\mathcal{T}(u)$ can be written in terms of the dimensionless parameter $u = k\tau$ and in presence of anisotropic stress is given by [5, 6]:

$$\mathcal{T}''(u) + 2\frac{da}{a du}\mathcal{T}'(u) + \mathcal{T}(u) = -24f_\nu(u)\left(\frac{da}{a du}\right)^2 \int_{u_{\text{dec}}}^u \frac{j_2(u-s)}{(u-s)^2}\mathcal{T}'(s)ds, \quad (2)$$

with primes denoting the derivative with respect to u . The value u_{dec} corresponds to the moment of neutrino decoupling, and the neutrino fraction f_ν of the total energy density

$$f_\nu = \frac{\Omega_\nu}{\Omega_\gamma + \Omega_\nu}[1 + a(\tau)/a_{\text{eq}}]^{-1} \quad (3)$$

is equal to 0.41 during radiation domination and gradually decreases after matter-radiation equality which happens at the value a_{eq} of the scale factor. Finally, $j_2(u)$ is the spherical Bessel function of the second kind. More details of the derivation that led to the above can be found in [5, 6].

The complexity of the integro-differential Eq. (2) requires building the solution independently for each k . We adopt an iterative approach: we start with the solution $\mathcal{T}^{(0)}(u)$ of the homogeneous part of Eq. (2), and then find the corrections $\mathcal{T}^{(n)}(u)$ driven by the integral term with $\mathcal{T}^{(n-1)}(u)$, such that

$$\mathcal{T}(u) = \mathcal{T}^{(0)} + \sum_{n=1}^N \mathcal{T}^{(n)}, \quad (4)$$

The initial conditions are given by:

$$\mathcal{T}^{(0)}(0) = 1, \quad \frac{d\mathcal{T}^{(0)}}{d\tau}(0) = 0, \quad \mathcal{T}^{(n)}(0) = 0, \quad \frac{d\mathcal{T}^{(n)}}{d\tau}(0) = 0, \quad n = 1, 2, \dots \quad (5)$$

Here, N denotes the number of iterations. This method has computational complexity $\mathcal{O}(N^2)$ for each mode k and stops when the correction reaches the required precision. For our purposes, the percent-level precision suffices, achieved with $N \lesssim 10$.

The differential operator of Eq. (2) leads to oscillatory functions similar to Bessel functions, whose oscillations make integration up to large u computationally expensive. To deal with this, we integrate numerically up to some sufficiently large cut-off $u_{\text{end}} = 200$ that covers many oscillations. The solution $\mathcal{T}(u)$ for larger u is then matched with the WKB approximation [6, 7, 36]:

$$\mathcal{T}(u) = A(u) \sin(u + \delta), \quad A(u) = A_0 \frac{a(\tau_{\text{end}})}{a(u/k)}. \quad (6)$$

The amplitude A_0 can be extracted by matching the numerical solution to the analytic formula at the end of the integration:

$$A_0 = \sqrt{\mathcal{T}^2(u_{\text{end}}) + \mathcal{T}'^2(u_{\text{end}})}. \quad (7)$$

The standard expression for the PGW spectral energy density of $\Omega_{\text{GW}}(\tau, k)$ is then given by [6]:

$$\Omega_{\text{GW}}(\tau, k) = \frac{\Delta_{\text{GW,prim}}^2}{12H^2(\tau)a^2} [\mathcal{T}'(\tau, k)]^2, \quad (8)$$

where the normalization factor $\Delta_{\text{GW,prim}}^2$ is defined by the primordial input spectrum. Presuming an epoch of slow-roll single-field inflation to have preceded reheating, the amplitude of the primordial power spectrum at some characteristic pivot scale is given by $\Delta_{\text{GW,prim}}^2$ is [37, 38]:

$$\Delta_{\text{GW,prim}}^2 \equiv 4 \frac{k^3}{2\pi^2} |h_{\text{prim}}(k)|^2 = \frac{2}{\pi^2} \left(\frac{H_{\text{inf}}}{M_{\text{Pl}}} \right)^2, \quad (9)$$

TABLE I: Fiducial cosmological parameters adopted.

h	0.7
$\Omega_r h^2$	4.15×10^{-5}
Ω_m	$1 - \Omega_R$
H_{inf}	2.41×10^{13} GeV
T_{CMB}	2.34×10^{-4} eV
$T_{\nu, \text{dec}}$	2 MeV

where M_{Pl} refers to reduced Planck units $M_{\text{Pl}}^{-1} = 8\pi G_N$, and we adopt the same conventions of [6]. Given that the factor $\sin(u + \delta)$ implicit in Eq. (8) is a rapidly oscillating function, we plot and analyze only the amplitude $A(u)$ for various scenarios in what follows. The fiducial values of various cosmological parameters utilized in our calculations are provided in Table I. Here, h denotes the dimensionless Hubble parameter, Ω_r and Ω_m are relative energy densities of radiation and matter, H_{inf} is the Hubble parameter at the end of inflation, and T_{CMB} is the current temperature of the CMB, and $T_{\nu, \text{dec}}$ is the neutrino decoupling temperature.

III. EARLY MATTER DOMINATION

There are multiple distinct scenarios in which one or more intervals of matter domination intersperse an initial and terminal stage of radiation domination, with the initial stage corresponding to reheating, and the terminal stage corresponding to the epoch preceding BBN [39]. Each scenario will result in a distinct late time spectral density depending on the number and relative duration of the matter domination phases. Nevertheless, one can infer certain general features by examining a representative example, the most notable of which is the fact that the high frequency plateau of the spectral density will be suppressed relative to the standard thermal history.

One such scenario is a massive field ϕ that drives reheating (whether it be the inflaton itself or one of its decay products) and decays into Standard Model quanta afterwards [40, 41] with an intervening epoch matter domination being the result. We assume that the universe is dominated by radiation, and ϕ behaves as radiation with relative energy contribution Ω_ϕ until the temperature drops below the mass of the field m_ϕ . After that, the dynamics of two dominant components, radiation and the inflaton field ϕ , during the EMD, is described by the coupled Boltzmann equations:

$$\frac{d\rho_\phi}{dt} + 3H\rho_\phi = -\Gamma_\phi\rho_\phi, \quad (10)$$

$$\frac{d\rho_R}{dt} + 4H\rho_R = \Gamma_\phi\rho_\phi, \quad (11)$$

where ρ_ϕ and ρ_R are energy densities of ϕ and the radiation fluid, H is the Hubble parameter, and where Γ_ϕ is the decay width of ϕ quanta.

The decay width Γ_ϕ can be expressed in terms of reheating temperature T_{reh} [42–44]:

$$\Gamma_\phi = \sqrt{\frac{4\pi^3 g_\star(T_{\text{reh}})}{45} \frac{T_{\text{reh}}^2}{M_{\text{Pl}}}}, \quad (12)$$

where $g_\star(T)$ is the effective number of relativistic degrees of freedom contributing to the radiation energy density, and M_{Pl} is the Planck mass. The value of T_{reh} is constrained by BBN: $T_{\text{reh}} \gtrsim T_{\text{BBN}} \sim 4$ MeV [45–48].

The evolution of the temperature (which we denote as T) can be solved in terms of the scale factor a as:

$$\frac{dT}{da} = \left[1 + \frac{T}{3g_{*,s}} \frac{dg_{*,s}}{dT} \right]^{-1} \left[-\frac{T}{a} + \frac{\Gamma_\phi \rho_\phi}{3H(a)s_R(T)a} \right], \quad (13)$$

where $g_{*,s}(T)$ is the effective number of relativistic degrees of freedom contributing to the entropy of the relativistic component $s_R(T)$.

In the simple case, where the number of relativistic degrees of freedom g_* [40] remains constant, we have:

$$\rho_R \sim \begin{cases} a^{-4} & \text{for } a \ll a_{\text{start}}, \\ a^{-\frac{3}{2}} & \text{for } a_{\text{start}} \ll a \ll a_{\text{reh}}, \\ a^{-4} & \text{for } a_{\text{reh}} \ll a, \end{cases} \quad (14)$$

and

$$T(a) \sim \begin{cases} a^{-1} & \text{for } a \ll a_{\text{start}}, \\ a^{-\frac{3}{8}} & \text{for } a_{\text{start}} \ll a \ll a_{\text{reh}}, \\ a^{-1} & \text{for } a_{\text{reh}} \ll a, \end{cases} \quad (15)$$

where a_{start} and a_{reh} are the scale factors at the start of EMD and reheating. Figure 1 demonstrates how temperature evolves for the reheating field mass $m_\phi = 2$ GeV, decay width $T_{\text{reh}} = 40$ MeV, and $\Omega_\phi/\Omega_r = 1\%$.

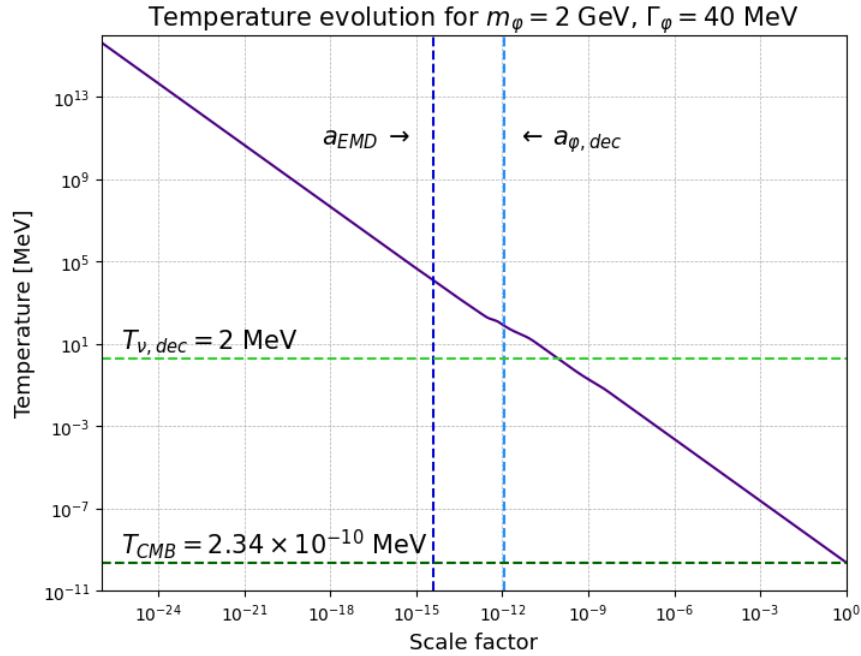


FIG. 1: Temperature evolution as a function of scale factor in the model with EMD induced by $m_\phi = 2$ GeV particle with decay width $T_{\text{reh}} = 40$ MeV. Dashed vertical lines mark start of EMD a_{EMD} and reheating $a_{\phi, \text{dec}}$. Dashed horizontal lines represent the temperatures at neutrino $T_{\nu, \text{dec}} = 2$ MeV and the present CMB temperature $T_{\text{CMB}} = 2.34 \cdot 10^{-10}$ MeV.

The effect of this new field on the spectrum is determined by two parameters: the reheating field mass m_ϕ and its decay width Γ_ϕ that control respectively the beginning and the end of the EMD phase.

Figure 2 depicts a scenario where $m_\phi = 2$ GeV and $\Gamma_\phi = 40$ MeV. Figure 1 depicts T as a function of scale factor a for the same parameters, while the PGW spectral density is plotted in Figure 3.

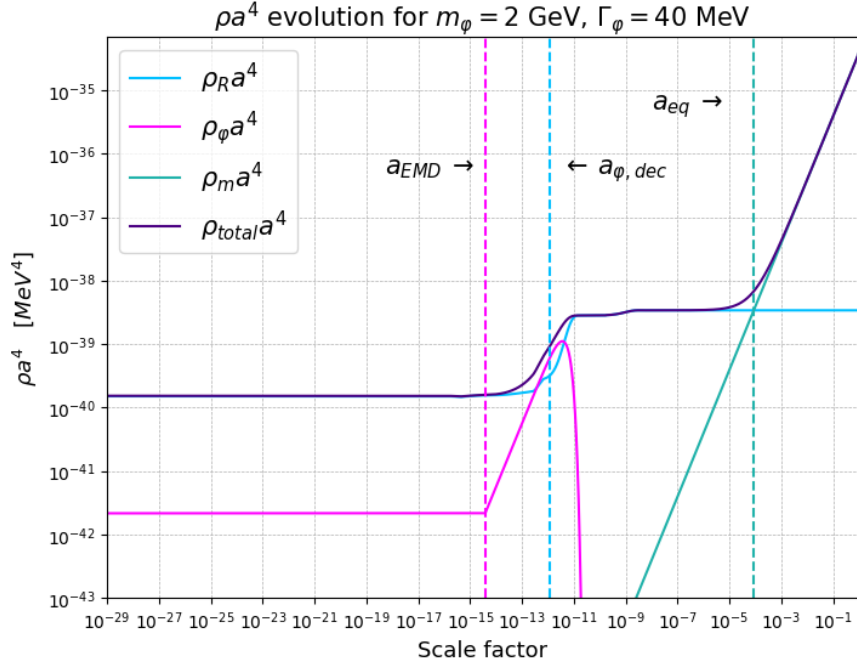


FIG. 2: Evolution of the energy density ρa^4 as a function of the scale factor in a model with EMD induced by $m_\phi = 2$ GeV particle with decay width $T_{\text{reh}} = 40$ MeV. Solid lines represent radiation (blue), ϕ (magenta), matter (green), and the total energy density of the Universe (indigo). Dashed vertical lines indicate transitions to EMD (magenta), reheating (blue), and MD (green).

All plots exhibit a distinct step-like feature caused by the energy transfer from the ϕ field to radiation. This property appears in all considered models with massive unstable particles. The width and height of the step depend on m_ϕ , Γ_ϕ , and ρ_R/ρ_ϕ and can be understood analytically. Before discussing this, it is useful to first provide the scaling relations for the gravitational wave energy density Ω_{GW} during the matter and radiation domination. In the absence of anisotropic stresses, a solution to Eq. (2) is simply expressed in terms of Bessel functions [6, 7, 36]. Consequently, the energy spectrum of PGWs can be written as:

$$\Omega_{\text{GW}}(\tau, k) \sim (a(\tau_{\text{h.c.}})k)^2 = (a(k^{-1})k)^2, \quad (16)$$

where $a(\tau_{\text{h.c.}})$ is the scale factor at the time of horizon crossing. This relation holds for a constant equation of state and for wave modes with $k \gg \tau_0^{-1}$, where τ_0 is the present conformal time. During the RD, the scale factor behaves as $a \propto \tau \propto 1/k$, resulting in a constant spectrum $\Omega_{\text{GW}} = \text{const.}$ On the other hand, during MD, the scale factor is $a \propto \tau^2 \propto 1/k^2$, resulting in a decreasing spectrum $\Omega_{\text{GW}} \sim k^{-2}$. The equation Eq. (16) can be generalized for an arbitrary equation of state ω that dominates the energy density as [6, 49]:

$$\Omega_{\text{GW}}(\tau, k) \sim k^{\frac{2(3\omega-1)}{1+3\omega}}. \quad (17)$$

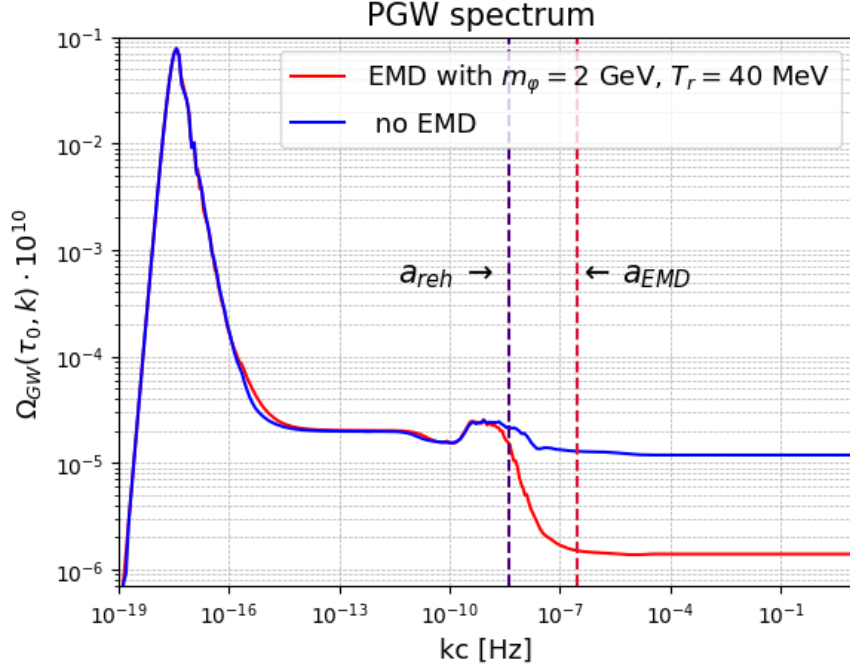


FIG. 3: Spectrum of primordial gravitational waves at $\tau = \tau_0$ as the function of comoving wavelength k (frequency kc in Hz). The blue line corresponds to the conventional RD, red describes the scenario with EMD induced by $m_\phi = 2$ GeV particle with reheating temperature $T_{\text{reh}} = 40$ MeV. Dashed vertical lines mark the start of the EMD (red) and reheating (blue).

To isolate the influence of the mass of the ϕ on the suppression of PGW spectrum, we fix Γ_ϕ and use the definition of $\Omega_{\text{GW}}(\tau, k)$ and energy density evolution laws to obtain:

$$\Omega_{\text{GW}}(\tau, k) = \frac{\tilde{\rho}_{\text{GW}}(\tau, k)}{\rho(\tau)} \sim \frac{a^{-4}}{m_\phi a^{-3}} \sim \frac{a^{-1}}{m_\phi} \quad (18)$$

during matter domination. This implies that the suppression is inversely proportional to m_ϕ . The heavier the ϕ field, the faster the expansion of the Universe and the greater the suppression of the tail. In addition, m_ϕ determines the beginning of the phase of EMD. In terms of comoving wavelength:

$$k_{\text{EMD}} \sim a_{\text{EMD}}^{-1/2} \sim \left(\frac{T_{\text{EMD}}}{T_{\text{reh}}} \right)^{1/2} \sim \left(\frac{m_\phi}{T_{\text{reh}}} \right)^{1/2}. \quad (19)$$

Hence, k_{EMD} can be calculated using only the characteristics of ϕ , as they are the only dimensional parameters in the model. The decay width Γ_ϕ controls the reheating temperature, as $T_{\text{reh}} \sim \sqrt{\Gamma_\phi M_{\text{Pl}}}$ neglecting the change in g_* . Fixing the mass m_ϕ , and using the temperature evolution during RD and EMD described by Eq. (15), we find:

$$k_{\text{reh}} = \frac{\tau_0}{\tau_{\text{reh}}} k_0 = \frac{a_0}{a_{\text{reh}}} k_0 = \frac{T_{\text{reh}}}{T_{\text{CMB}}} k_0 = C(T_{\text{reh}}) \frac{\sqrt{\Gamma_\phi M_{\text{Pl}}}}{T_{\text{CMB}}} k_0, \quad (20)$$

$$k_{\text{EMD}} = \frac{\tau_{\text{reh}}}{\tau_{\text{EMD}}} k_{\text{reh}} = \left(\frac{a_{\text{reh}}}{a_{\text{EMD}}} \right)^{1/2} k_{\text{reh}} = \frac{T_{\text{EMD}}^{4/3}}{T_{\text{reh}}^{1/3} T_{\text{CMB}}} k_0 = \frac{C^{-1/3} (T_{\text{reh}}) m_\phi^{4/3}}{\Gamma_\phi^{1/6} M_{\text{Pl}}^{1/6} T_{\text{CMB}}} k_0, \quad (21)$$

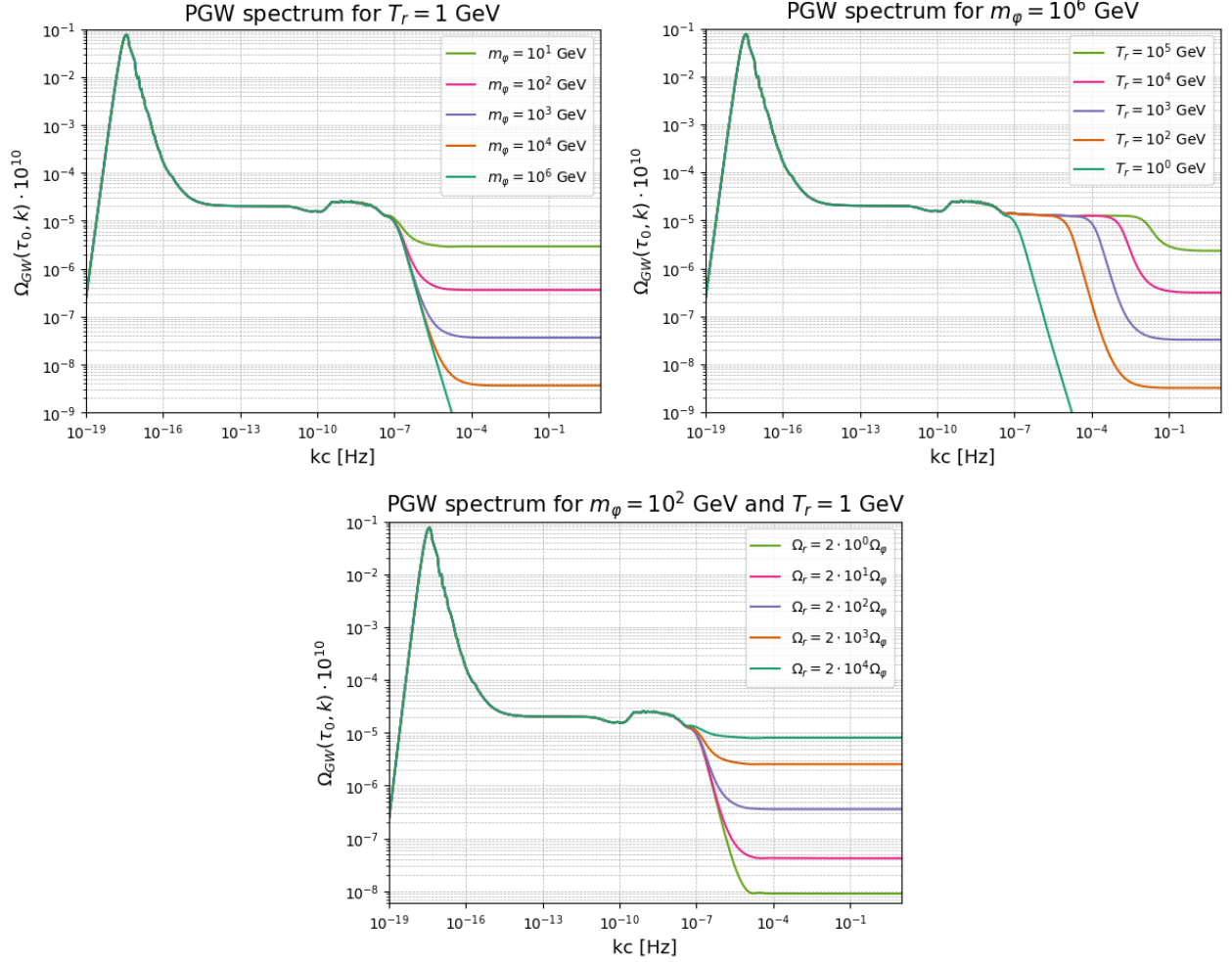


FIG. 4: Spectra of primordial gravitational waves at $\tau = \tau_0$ as functions of comoving wavelength k , for varied particle mass m_ϕ (left top), reheating temperature T_r (right top), and the initial radiation-to- ϕ ratio Ω_ϕ/Ω_r . The default parameters are $m_\phi = 10^6$ GeV, $T_r = 1$ GeV, and $\Omega_\phi = 5 \cdot 10^{-3} \Omega_r$.

where $k_0 = \tau_0^{-1}$ is the present day value, and the constant $C(T_{\text{reh}})$ is:

$$C(T_{\text{reh}}) = \left(\frac{45}{4\pi^3 g_*(T_{\text{reh}})} \right)^{1/4}. \quad (22)$$

Therefore, a larger decay width results in earlier reheating. Shifts in the beginning of the EMD can be attributed to changes in initial conditions due to rescaling to match the observed radiation energy density. The magnitude of the suppression factor μ can be expressed as a function of both m_ϕ and Γ_ϕ :

$$\mu = \frac{\Omega_{\text{GW}}^{\text{EMD}}}{\Omega_{\text{GW}}^{\text{reh}}} = \frac{a_{\text{reh}}}{a_{\text{EMD}}} = \left(\frac{m_\phi^2}{\Gamma_\phi M_{\text{Pl}}} \right)^{2/3}. \quad (23)$$

We see that the longer the lifetime of the particles (i.e. the smaller the decay width) and the higher their masses, the greater the suppression of the high frequency tail. In the calculation above, we

assumed that ρ_ϕ constitutes $\sim 1\%$ of the initial energy density as a realistic scenario. However, one can vary this parameter as well. Figure 4 shows results for different initial Ω_r/Ω_ϕ ratios, where ϕ is always subdominant. A more precise expression for the beginning of EMD, which accounts for the energy distribution between ϕ and radiation, is:

$$a_{\text{EMD}}^{\text{precise}} = \frac{\Omega_r^{\text{init}}}{\Omega_\phi^{\text{init}}} a_{\text{freeze-out}} , \quad (24)$$

where $a_{\text{freeze-out}}$ is the scale factor at freeze-out. The smaller the energy fraction of the ϕ field, the later it starts to dominate. For fixed m_ϕ and Γ_ϕ , the suppression is $\sim \Omega_r^{\text{init}}/\Omega_\phi^{\text{init}}$. As a result, measuring the magnitude of the suppression and EMD duration could facilitate inferring the mass and decay width of particles causing EMD, potentially excluding some new physics particles (e.g., heavy neutral leptons) not accessible to current and proposed collider experiments.

IV. LONG LIVED FEEBLY INTERACTING PARTICLES

Massive feebly interacting particles (FIPs) with long lifetimes feature in several beyond the Standard Model scenarios. Examples of FIPs include dark scalars, heavy neutral portals (HNLS), dark photons, and axion-like particles (ALPs) (see [50, 51] for an overview). Such particles have a variety of phenomenological motivations, and may even be within the experimental reach of future accelerator experiments [52, 53]. Depending on their lifetimes, they could also imprint on cosmological observables. If the FIPs in question interact feebly enough, a phase of EMD can be induced if all of the following conditions are met:

- The FIPs decouple while still being present with sufficient abundance in the primordial plasma. The decoupling temperature T_{fr} cannot be considerably lower than the FIP mass m , $T_{\text{fr}} \gtrsim m$, otherwise their number density becomes exponentially suppressed.
- The plasma temperature T_{dec} at the moment of FIP decay must have dropped to be substantially below the FIP mass $T_{\text{dec}} \ll m$.
- FIP decay and subsequent thermalization temperature T_{reh} must be above several MeV so as not to spoil the predictions of Big Bang Nucleosynthesis [54, 55]³.

For simple order-of-magnitude estimates as to whether the described scenario occurs, we assume that the FIP production rate scales with temperature as $\Gamma_{\text{prod}} \sim T^{n+1}/\Lambda^n$ once $T \gtrsim m$. The parameters Λ , n are determined by the particular phenomenological model. The time of freeze-out is given by $\Gamma(T) = H(T)$, or

$$T_{\text{fr}} \sim (\Lambda^n M_{\text{Pl}}^{-1})^{1/(n-1)}.$$

On the other hand, we can make a similar estimate for the FIP decay rate by replacing the temperature with the particle mass m : $\Gamma_{\text{decay}} \sim m^{n+1}/\Lambda^n$. This is a reasonable assumption if there are no dominant decays into some exotic dark sector that does not contribute to the FIP production rate. Once the FIPs become nonrelativistic, the universe enters an epoch of matter-domination $H(T) \sim \sqrt{mT^3}/M_{\text{Pl}}$, and the decay temperature reads

$$T_{\text{dec}} \sim m \times \left(\frac{m}{T_{\text{fr}}} \right)^{\frac{2}{3}(n-1)}.$$

³ Although not relevant to the scenarios we consider, FIPs that live long enough to decay in the window of redshift $z \sim 10^6$ and 10^3 do so in an epoch when Compton scattering in the primordial plasma is not efficient enough to thermalize the decay products, imprinting a distortion of the cosmic microwave background spectrum [56].

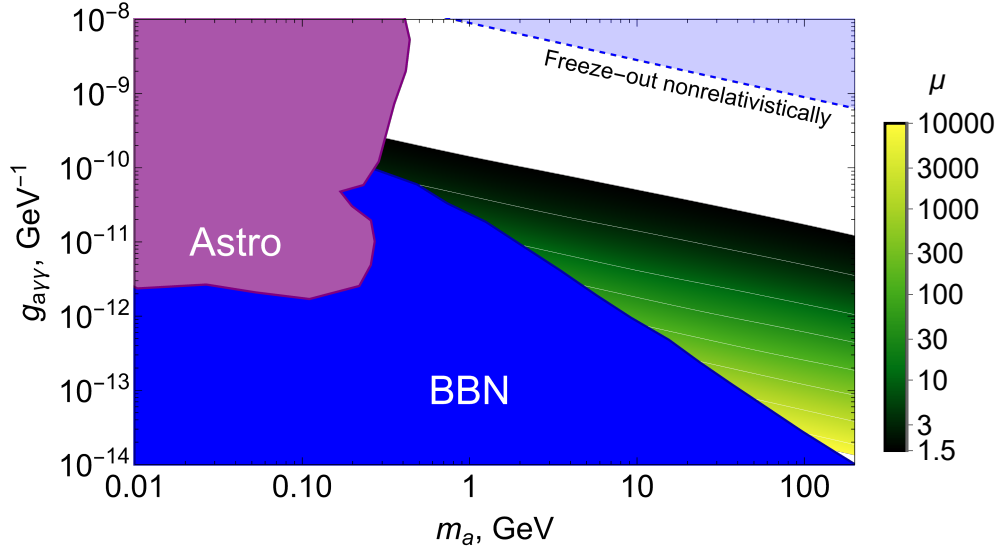


FIG. 5: The suppression factor μ in the parameter space of the photon-coupled ALP with the current cosmological and astrophysical constraints [57]. At higher $g_{a\gamma\gamma}$, interactions are too rapid, and ALPs effectively annihilate before freezing out.

The requirements for EMD – $T_{\text{dec}} \ll m \lesssim T_{\text{fr}}$ – can only be satisfied with $n > 1$, which excludes renormalizable interactions like those corresponding to dark scalars and dark photons. However, even if a phase of EMD can't be realized through the latter channels, changes in the number of relativistic species and bursts of anisotropic stress production can still induce imprints on the late time gravitational wave spectral density in certain scenarios. On the other hand, FIP species such as axion-like particles and heavy neutral leptons and indeed drive a phase of EMD below the electroweak scale with non-renormalizable effective interactions of the Fermi theory variety. We consider each separately.

Axion-like particles: We consider a model of an axion-like particle with a photon-dominant coupling (cf. the *BC9* model of [51]). Before electroweak symmetry breaking, the Lagrangian reads:

$$\mathcal{L}_a = \frac{1}{2} \partial_\mu a \partial^\mu a - \frac{m_a^2}{2} a^2 - \frac{g_{a\gamma\gamma}}{4 \cos^2 \theta_W} a B_{\mu\nu} \tilde{B}^{\mu\nu},$$

with a being the ALP field, and $B_{\mu\nu}$ being the field strength of the hypercharge group $\tilde{B}_{\mu\nu} = \frac{1}{4} \epsilon_{\mu\nu\lambda\rho} B^{\lambda\rho}$.

As long as the ALPs decouple while they are still relativistic, the exact cross-section of processes that maintain thermal equilibrium is not relevant, and the freeze-out temperature and the axion decay width are given simply by [54]:

$$T_{\text{fr}} \approx 100 \left(\frac{10^{-9} \text{ GeV}^{-1}}{g_{a\gamma\gamma}} \right)^2 \text{ GeV}, \quad \Gamma(a \rightarrow \gamma\gamma) = \frac{g_{a\gamma\gamma}^2 m^3}{64\pi}.$$

To find the high frequency tail suppression factor μ (derived in Eq. (23)), we numerically solve the Eqs. 10 and 11 for the energy density starting from the relativistic number density of axions. The resulting suppression scale for ALPs is shown in Fig. 5.

Heavy Neutral Leptons: HNLs [20–22] are an appealing extension of the Standard Model that can simultaneously account for the origin of neutrino masses via the seesaw mechanism [58–61] and the baryon asymmetry via leptogenesis [62–64]. The new particles mix with active neutrinos by a small mixing angle U_α , $\alpha = e, \mu, \tau$, which couple HNLs to the standard model via a weak-like interaction. To account for the neutrino masses, the mixing angles cannot be smaller than the seesaw bound

$$U_{\text{seesaw}}^2 \gtrsim \frac{m_\nu}{m_N},$$

where $m_\nu \sim \sqrt{\Delta m_{\text{atm}}^2} \sim 50$ meV is the scale of active neutrino masses and m_N is the HNL mass.

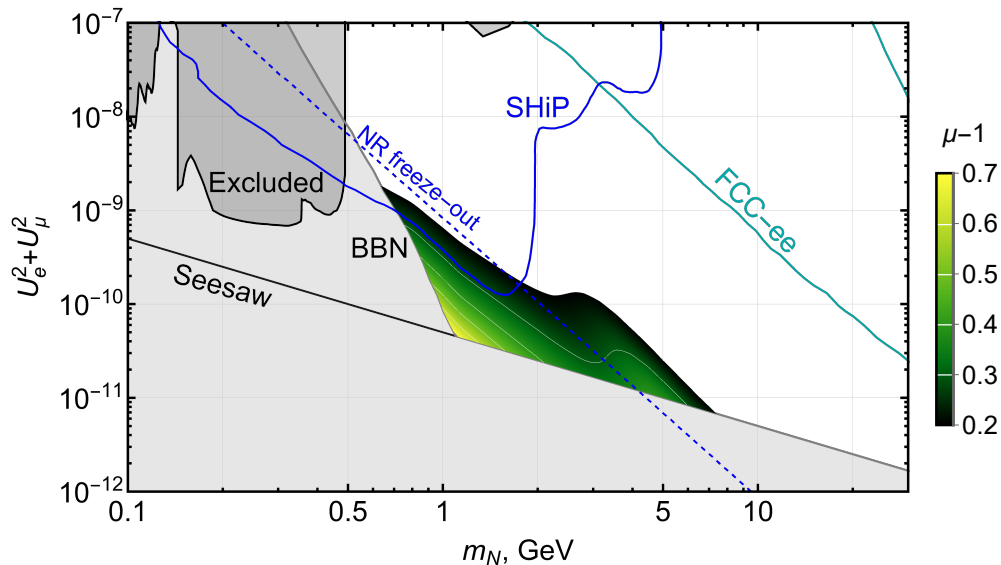


FIG. 6: The suppression factor μ in the parameter space of an HNL pair with electrons mixing is presumed to be the dominant channel. Filled regions are constraints from BBN [55, 65], direct searches [66], and the seesaw bound, while solid lines show the projected sensitivities of SHiP [67] and FCC-ee in the Z -pole mode [68]

Future experiments such as the planned SHiP experiment [69, 70] and the proposed FCC [68, 71, 72] aim to push the limits on the mixing angle at the GeV scale by orders of magnitude, but are incapable of closing the parameter space completely down to the seesaw bound. Therefore, complementary probes from below, such as BBN, are needed. The effect of HNLs on the spectrum of primordial GW offers a powerful probe to further constrain the unexplored parameter space.

As our findings indicate, the parameter space in which HNLs can drive an epoch of EMD covers the mass range of 1 – 10 GeV, outside of which such long-lived HNLs are excluded by either the BBN constraints or the seesaw bound. In this region, HNLs are on the verge of decoupling whilst still nonrelativistic, necessitating an accurate estimation of their abundance, which we obtain via the Boltzmann equation. HNLs interact mainly via processes of the form $N + \text{SM} \leftrightarrow \text{SM} + \text{SM}$. The rescattering channels $N + \text{SM} \leftrightarrow N + \text{SM}$ that preserve the HNL number but change its momentum require HNL-neutrino mixing to occur twice and are therefore doubly suppressed by the small mixing angle. Moreover, the weak interaction cross-section of HNLs exhibits a strong dependence on the center-of-mass energy. In light of these considerations, we opted for the following scheme: each momentum shell in the HNL phase space is treated as a separate system equilibrating with the SM thermal bath. Specifically, for the total number density $\Delta f(y)$ of HNLs in a spherical

momentum shell in the radius range $(y, y + \Delta y)$, where $y = p/T$ and p is the corresponding physical momentum, we solve the equation

$$\frac{d\Delta f(y)}{dt} = -3H\Delta f - \Gamma(yT)(\Delta f - \Delta f^{\text{eq}}),$$

where H is the Hubble parameter and $\Gamma(p) = \sum_{A \in \text{SM}} n_A \times \langle \sigma_{N+A}(p)v \rangle_{\text{th. average}}$ is the interaction rate summed over all species A and thermally averaged. The equilibrium number density Δf^{eq} per HNL is thus given by

$$\Delta f^{\text{eq}}(y) = \frac{T^3}{\pi^2} \frac{y^2 \Delta y}{\exp \sqrt{\frac{m_N^2}{T^2} + y^2} + 1}.$$

In our toy model, we assume that the universe is dominated by the following relativistic species at GeV temperatures: three neutrino species, electrons, muons, and light u, d, s . Heavier particles are highly subdominant, and the HNL contribution to the Hubble parameter is neglected. The interaction cross-section is computed precisely for each SM particle using the matrix elements from [73] and thermally averaged. For each momentum shell y , we track the evolution of the spectrum until the shell freezes out. The calculated final HNL abundance serves as the initial condition for the subsequent estimate of the EMD suppression factor μ (Eq. (23), plotted in Fig. 6).

The contours depicted on the plot presume two Majorana HNLs with equal total mixing angle U^2 , where for simplicity, tau neutrino mixing is presumed to be negligible. In the approximation where all light particles are taken to be relativistic, electrons and muons can be treated equivalently and the results depend only on the total mixing angle $U_e^2 + U_\mu^2$. A weakness and restriction of our modeling lies in the assumption that HNL decoupling and their subsequent decay during EMD are sufficiently separated in time. In the event that the interaction rate $\Gamma \sim G_F^2 T^5$ with the SM is strong enough to keep HNLs in equilibrium until they are nonrelativistic, decays with the rate $\Gamma \sim G_F^2 m_N^5$ are already active when decoupling is occurring. A more accurate modeling of the full dynamics that simultaneously accounts for both effects is needed to draw definitive conclusions.

Dark radiation: FIPs that are not sufficiently long-lived to drive a period of EMD may still leave an imprint in the spectrum through two effects: the change of the effective number of DOF and the generation of anisotropic components to the stress tensor. Naively, the contribution of any such FIPs is limited to the percent level given the large value of $g_* \sim 100$ at energies above the GeV scale. In this section, we illustrate a plausible possible scenario that avoids this restriction.

We consider a dark sector, made up of various additional particles, that only interacts with the SM through a light mediator, e.g., dark photon or scalar. For concreteness, we assume that the mediator is the dark photon A' and the Lagrangian is:

$$\mathcal{L} = \mathcal{L}_{\text{SM}} + \mathcal{L}_{\text{DS}} - \frac{1}{4} F'^{\mu\nu} F'_{\mu\nu} - \frac{\epsilon}{2} F^{\mu\nu} F'_{\mu\nu} + \frac{m_{A'} A'^2}{2} + A'_\mu J_{\text{DS}}^\mu \quad (25)$$

with \mathcal{L}_{SM} , \mathcal{L}_{DS} are Lagrangians of the Standard Model and the dark sector respectively, $F_{\mu\nu}$ and $F'_{\mu\nu}$ are the field tensors of the ordinary and dark photon, whose kinetic mixing is parameterized by the dimensionless coupling ϵ . From the comparison of the equilibration rate between the dark sector and the SM $\Gamma_{\text{eq}} \sim \alpha \epsilon^2 T$ with the expansion rate $H \sim T^2/M_{\text{Pl}}$, it is evident that the two sectors evolve independently at sufficiently high temperature. Therefore, it is not unreasonable to assume that the associated energy densities of the two sectors are unrelated. In our model, we make the following assumptions:

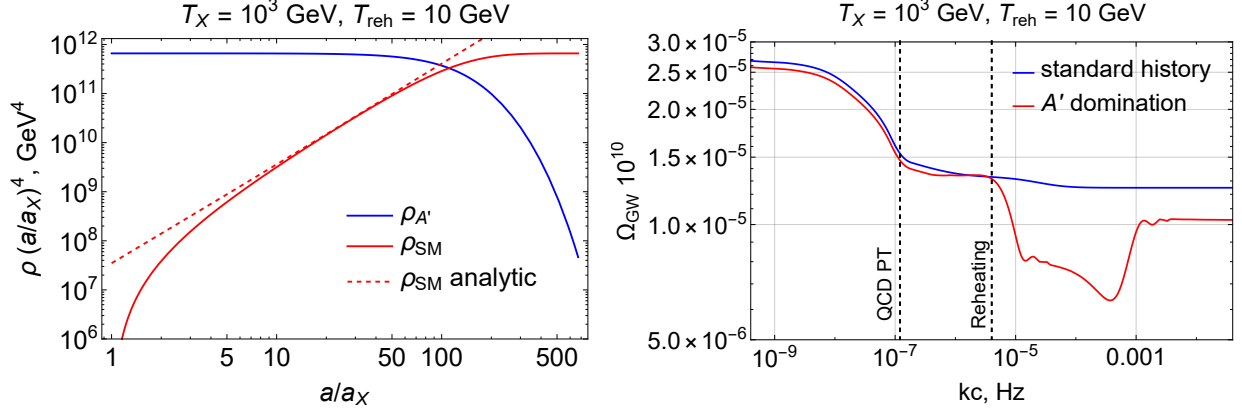


FIG. 7: Left: energy transfer from dark photons into the SM. Right: the comparison of the GW spectra for the standard thermal history and early dark radiation. The height of the right plateau depends on the concrete composition of the dark sector. For the sake of concreteness, we assume that the species X is a scalar and other possible particles are much heavier.

- The dark sector initially dominates the energy budget of the universe
- The mass of the lightest ‘dark charged’ particle X of the dark sector is larger than that of dark photon A'
- Annihilation of X happens before the interaction rate between A' and the SM becomes sufficient to equilibrate the two sectors

After X annihilates at temperature, given roughly by

$$T_X \sim \frac{m_X}{\ln[\alpha_D^2 M/m_X]} \sim \frac{m_X}{20},$$

the universe becomes populated with a gas of decoupled dark photons A' and a small admixture of the SM. Rare interactions between them, such as $eA' \rightarrow e\gamma$, slowly convert the energy stored in dark photons into the SM plasma. Given that the interaction in the SM plasma is always rapid enough to keep the plasma in equilibrium, the conversion can be described via the system of equations:

$$\frac{d\rho_{A'}}{dt} = -4H\rho_{A'} - \rho_{A'} \langle n_{\text{SM}} \sigma(T_{A'}, T_{\text{SM}}) \rangle \quad (26)$$

$$\frac{d\rho_{\text{SM}}}{dt} = -3H(\rho_{\text{SM}} + p_{\text{SM}}) + \rho_{A'} \cdot \langle n_{\text{SM}} \sigma(T_{A'}, T_{\text{SM}}) \rangle \quad (27)$$

with the dark photon temperature $T'_A = T_X \cdot a_X/a$ following the standard redshift, while the SM plasma temperature T_{SM} is determined by energy density $\rho_{\text{SM}} \equiv \pi^2 g_* T^4/30$. We do not include the energy transfer due to decay of dark photons, as we have found it to be a subdominant process as long as $\epsilon^2 \gtrsim m_{A'}/M_{\text{Pl}}$. The remaining integrated collision terms are given by the averaged interaction cross-section:

$$\langle n_{\text{SM}} \sigma \rangle \sim \epsilon^2 \frac{\zeta(3)}{\pi^2} T_{\text{SM}}^3 \times \frac{4\pi\alpha^2}{3s} \sum_{i \in \text{SM}} g_{n,i} Q_i^2$$

in which we neglect possible logarithmic enhancement factors in the cross-section and crudely assume $s \sim 4T_{\text{SM}}T_{A'}$.

The solutions of the equations Eq. (26) have a number of analytic features. From any initial nonzero seed, the SM energy density quickly approaches the value

$$\rho_{\text{SM}}(a) = \rho_0 \left(\frac{a_X}{a} \right)^2, \quad \rho_0 = \left[\epsilon^2 \frac{M_{\text{Pl}} T_X}{\sqrt{2 \frac{8\pi}{3} g_*(T_{\text{SM}})}} \frac{\zeta(3)}{\pi^2} \frac{\pi \alpha^2}{3} \sum g_{n,i} Q_i^2 \right]^2$$

during the expansion by a factor of $a/a_X \sim e$, as shown in the left panel of Fig. 7. By equating $\rho_{\text{SM}} \sim a^{-2}$ to $\rho_{A'} \sim a^{-4}$, one can estimate the effective temperature of dark photons at the moment of SM equilibration:

$$T_{\text{reh}} \sim 1.4 \text{ GeV} \times \frac{\epsilon^2}{10^{-7}}$$

To recap: in this scenario, the universe has a phase of domination by *decoupled radiation* from the temperature T_X down to the reheating temperature T_{reh} . Gravitational waves that enter the horizon during this epoch are affected by the anisotropic stress tensor of the decoupled A' quanta, after which dark radiation gets rapidly converted into SM particles and precipitates the terminal phase of radiation domination. To quantify the damping effects of this burst of anisotropic stress production, we use the same approach as used for Eq. (2) for free streaming neutrinos. The fraction f of the energy density of decoupled radiation is unit in the temperature range $[T_{\text{reh}}, T_X]$ and vanishes otherwise. The numerical solution of the equation indicates that the energy density of PGWs that enter the horizon during the dark radiation period becomes suppressed by roughly 60%, as illustrated in Figure 7.

This is perhaps the most striking of all the features generated in the various scenarios we've considered in our survey – although a number of scenarios consider the gravitational wave spectrum generated by an epoch of dark radiation [31–33, 74, 75], bursts of anisotropic stress production can occur in various scenarios in certain regions of parameter space and have to be factored into the transfer function for accurate predictions for the late time spectral density.

V. KINATION

Another plausible non-standard thermal history is provided by kination (KD), where the kinetic energy of a scalar field dominates the energy density of the universe at some epoch following on from a phase of EMD. In this section, we consider a specific model of axion kination described in [49, 76], where inflation is followed by Standard Model radiation domination. The contribution of the axion field ϕ to ρ_{tot} is minor immediately after reheating, and remains constant until the expansion rate becomes smaller than the mass of the axion field m_s . At this juncture, the axion begins to oscillate around the minimum of its potential and the spatial zero mode has the time averaged equation of state of cold dark matter, wherein a phase of EMD onsets. Kination commences once the potential energy of ϕ falls to below its kinetic energy. In this regime, the energy density of the Universe decreases as $\rho_{\text{tot}} \sim a^{-6}$, which is faster than that of radiation, and a terminal phase of radiation domination occurs after $\rho_R \approx \rho_\phi$. Approximating each of these regimes in a piece-wise manner [77], one can show that the Hubble parameter $H(T)$ evolves as:

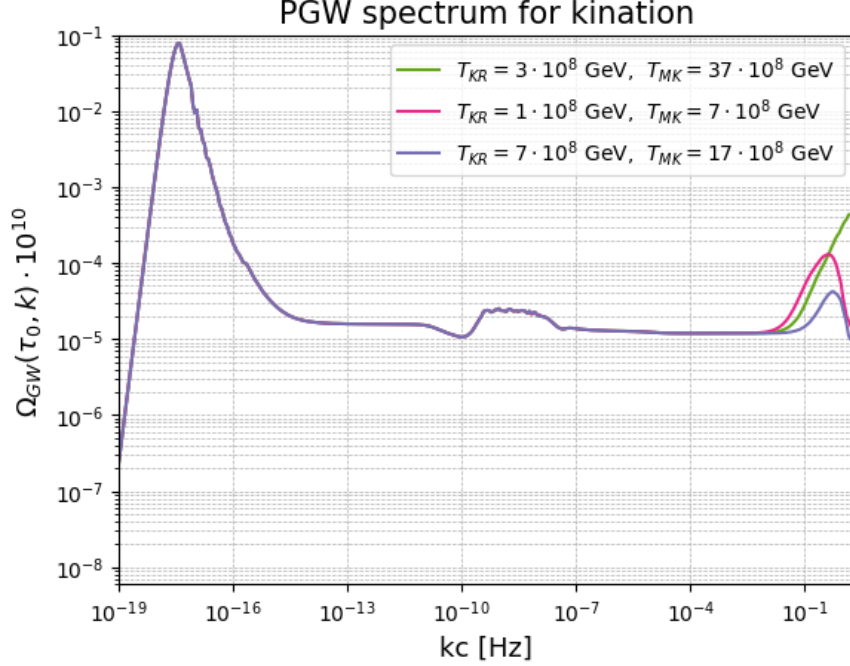


FIG. 8: Spectra of primordial gravitational waves at $\tau = \tau_0$ as functions of comoving wavelength k , for varied axion parameters: $m_S = 10^7$ GeV and $f_a = 10^{10}$ GeV (green), $m_S = 3 \cdot 10^4$ GeV and $f_a \approx 10^9$ GeV (magenta), $m_S = 7 \cdot 10^5$ GeV and $f_a = 10^8$ GeV (purple).

$$H(T) \sim \begin{cases} T^2 & \text{for RD : } T \gg T_{RM}, \\ T_{RM}^2 \left(\frac{T}{T_{RM}} \right)^{\frac{3}{2}} & \text{for MD : } T_{RM} \gg T \gg T_{MK}, \\ T_{KR}^2 \left(\frac{T}{T_{KR}} \right)^3 & \text{for KD : } T_{MK} \gg T \gg T_{KR}, \\ T^2 & \text{for RD : } T_{KR} \gg T, \end{cases} \quad (28)$$

Where T_{RM} is the temperature at the beginning of EMD, T_{MK} is the temperature at the beginning of KD, and T_{KR} is the temperature at the end of kination epoch.

The allowed window for kination is quite large. Because EMD ends without entropy injection, EMD and KD can occur even after the BBN, although it must still occur before recombination. The cosmological constraints on the T_{RM} and T_{KR} are provided in [49, 77].

To determine the PGW spectrum, we utilize the piece-wise approximation Eq. (28) and keep all the standard cosmological parameters as indicated in Table I. Values of T_{RM} and T_{KR} were extracted from Co et al. (2022), while T_{MK} was calculated via

$$T_{MK} = T_{RM}^{\frac{1}{3}} T_{KR}^{\frac{2}{3}}. \quad (29)$$

We evaluated the spectral density only for early kination (occurring before BBN) and used temperatures allowing lepto-ALPgenesis with various axion field masses m_S and vacuum field values f_a . Those parameters are chosen to explain the observed baryon asymmetry by lepto-ALPgenesis for illustrative purposes. The results are shown in Figure 8 where a clear peak in the PGW spectrum is evident, consistent with the findings of [49, 77]. The relation Eq. (29) ensures that the high

frequency plateau that onsets after the peak in the spectrum will be at the same power as the plateau for modes that re-enter the horizon during the terminal stage of radiation domination. It has been noted that in principle, an enhanced high frequency plateau can result if the equation of state parameter transitions from the initial phase of radiation domination post-reheating directly to a phase of kination [35]. It would be interesting to investigate the spectrum that would result from a background model construction that consistently actualizes this.

VI. CONCLUDING REMARKS

This investigation has surveyed the implications for the late time spectral density of gravitational waves for a range of phenomenologically motivated scenarios of non-standard thermal histories. In addition to corroborating the findings of a range of studies via a detailed transfer function analysis, we have also uncovered the novel possibility of damping at intermediate scales via bursts of anisotropic stress production in scenarios involving dark photon production. Realistic detection prospects, either through pulsar timing arrays [78–80] or next generation interferometry [81, 82] hinge on an enhanced signal at the relevant frequency ranges, and hence only meaningfully place scenarios involving kination, first order phase transitions, or secondary gravitational wave production within reach of near term observations. Nevertheless, it is informative to place targets on longer term [83], possibly even tabletop experimental efforts [84]. That it is not just in principle, but rather practically possible to directly probe cosmological epochs that precede nucleosynthesis is a remarkable feature of gravitational wave cosmology, one that we hope will be in the realm of the actual within the lifetime of some of our readers.

VII. ACKNOWLEDGMENTS

We wish to thank Jens Chluba, Wolfram Ratzinger, and Pedro Schwaller for their comments on the manuscript. OM acknowledges funding from the European Research Council (ERC) under the European Union’s Horizon 2020 research and innovation programme (GA 694896), from the NWO Physics Vrij Programme “The Hidden Universe of Weakly Interacting Particles”, No. 680.92.18.03, which is partly financed by the Dutch Research Council NWO.

-
- [1] Michele Maggiore. Gravitational wave experiments and early universe cosmology. *Phys. Rept.*, 331:283–367, 2000.
 - [2] Chiara Caprini and Daniel G. Figueroa. Cosmological Backgrounds of Gravitational Waves. *Class. Quant. Grav.*, 35(16):163001, 2018.
 - [3] Gordon Baym, Subodh P. Patil, and C. J. Pethick. Damping of gravitational waves by matter. *Phys. Rev. D*, 96(8):084033, 2017.
 - [4] Raphael Flauger and Steven Weinberg. Gravitational Waves in Cold Dark Matter. *Phys. Rev. D*, 97(12):123506, 2018.
 - [5] Steven Weinberg. Damping of tensor modes in cosmology. *Phys. Rev. D*, 69:023503, 2004.
 - [6] Yuki Watanabe and Eiichiro Komatsu. Improved calculation of the primordial gravitational wave spectrum in the standard model. *Physical Review D*, 73(12):123515, 2006.
 - [7] Thomas Kite, Jens Chluba, Andrea Ravenni, and Subodh P. Patil. Clarifying transfer function approximations for the large-scale gravitational wave background in Λ CDM. *Mon. Not. Roy. Astron. Soc.*, 509(1):1366–1376, 2021.
 - [8] Alexander C. Jenkins and Mairi Sakellariadou. Anisotropies in the stochastic gravitational-wave background: Formalism and the cosmic string case. *Physical Review D*, 98(6), September 2018.

- [9] Giulia Cusin, Irina Dvorkin, Cyril Pitrou, and Jean-Philippe Uzan. Properties of the stochastic astrophysical gravitational wave background: Astrophysical sources dependencies. *Physical Review D*, 100(6), September 2019.
- [10] Giulia Cusin, Cyril Pitrou, and Jean-Philippe Uzan. Anisotropy of the astrophysical gravitational wave background: Analytic expression of the angular power spectrum and correlation with cosmological observations. *Physical Review D*, 96(10), November 2017.
- [11] Carlo R. Contaldi. Anisotropies of gravitational wave backgrounds: A line of sight approach. *Physics Letters B*, 771:9–12, August 2017.
- [12] Nicola Bartolo, Daniele Bertacca, Sabino Matarrese, Marco Peloso, Angelo Ricciardone, Antonio Riotto, and Gianmassimo Tasinato. Characterizing the cosmological gravitational wave background: Anisotropies and non-gaussianity. *Physical Review D*, 102(2), July 2020.
- [13] Nicola Bartolo, Daniele Bertacca, Robert Caldwell, Carlo R. Contaldi, Giulia Cusin, Valerio De Luca, Emanuela Dimastrogiovanni, Matteo Fasiello, Daniel G. Figueroa, Gabriele Franciolini, Alexander C. Jenkins, Marco Peloso, Mauro Pieroni, Arianna Renzi, Angelo Ricciardone, Antonio Riotto, Mairi Sakellariadou, Lorenzo Sorbo, Gianmassimo Tasinato, Jesús Torrado, Sebastien Clesse, and Sachiko Kuroyanagi. Probing anisotropies of the stochastic gravitational wave background with lisa. *Journal of Cosmology and Astroparticle Physics*, 2022(11):009, November 2022.
- [14] L. Valbusa Dall’Armi, A. Ricciardone, N. Bartolo, D. Bertacca, and S. Matarrese. Imprint of relativistic particles on the anisotropies of the stochastic gravitational-wave background. *Physical Review D*, 103(2), January 2021.
- [15] Giulia Cusin, Irina Dvorkin, Cyril Pitrou, and Jean-Philippe Uzan. First predictions of the angular power spectrum of the astrophysical gravitational wave background. *Physical Review Letters*, 120(23), June 2018.
- [16] Daniele Bertacca, Angelo Ricciardone, Nicola Bellomo, Alexander C. Jenkins, Sabino Matarrese, Alvis Raccanelli, Tania Regimbau, and Mairi Sakellariadou. Projection effects on the observed angular spectrum of the astrophysical stochastic gravitational wave background. *Physical Review D*, 101(10), May 2020.
- [17] Alice Garoffolo. Wave-optics limit of the stochastic gravitational wave background. *Phys. Dark Univ.*, 44:101475, 2024.
- [18] Anna Balaudo, Alice Garoffolo, Matteo Martinelli, Suvodip Mukherjee, and Alessandra Silvestri. Prospects of testing late-time cosmology with weak lensing of gravitational waves and galaxy surveys. *JCAP*, 06:050, 2023.
- [19] Ginevra Braga, Alice Garoffolo, Angelo Ricciardone, Nicola Bartolo, and Sabino Matarrese. Proper time path integrals for gravitational waves: an improved wave optics framework. 5 2024.
- [20] Takehiko Asaka and Hisashi Okui. Neutrino masses and gravitational wave background. *Phys. Lett. B*, 814:136074, 2021.
- [21] Maximilian Berbig and Anish Ghoshal. Impact of high-scale Seesaw and Leptogenesis on inflationary tensor perturbations as detectable gravitational waves. *JHEP*, 05:172, 2023.
- [22] Satyabrata Datta and Rome Samanta. Fingerprints of GeV scale right-handed neutrinos on inflationary gravitational waves and PTA data. *Phys. Rev. D*, 108(9):L091706, 2023.
- [23] Zafri A. Borboruah, Anish Ghoshal, Lekhika Malhotra, and Urjit Yajnik. Inflationary Gravitational Wave Spectral Shapes as test for Low-Scale Leptogenesis. 5 2024.
- [24] Nahuel Mirón-Granese. Relativistic viscous effects on the primordial gravitational waves spectrum. *JCAP*, 06:008, 2021.
- [25] Yuchao Gu, Liangliang Su, Lei Wu, Yongcheng Wu, and Bin Zhu. Gravitational wave as a probe of light feebly interacting dark matter. *Phys. Rev. D*, 110(1):015022, 2024.
- [26] Francesco D’Eramo and Kai Schmitz. Imprint of a scalar era on the primordial spectrum of gravitational waves. *Phys. Rev. Research.*, 1:013010, 2019.
- [27] W. Buchmuller, V. Domcke, K. Kamada, and K. Schmitz. A Minimal Supersymmetric Model of Particle Physics and the Early Universe. pages 47–77, 2013.
- [28] Varun Sahni and Limin Wang. New cosmological model of quintessence and dark matter. *Physical Review D*, 62(10):103517, 2000.
- [29] Wayne Hu, Rennan Barkana, and Andrei Gruzinov. Cold and fuzzy dark matter. *Phys. Rev. Lett.*, 85:1158–1161, 2000.

- [30] Lam Hui, Jeremiah P. Ostriker, Scott Tremaine, and Edward Witten. Ultralight scalars as cosmological dark matter. *Phys. Rev. D*, 95(4):043541, 2017.
- [31] Camila S. Machado, Wolfram Ratzinger, Pedro Schwaller, and Ben A. Stefanek. Audible Axions. *JHEP*, 01:053, 2019.
- [32] Camila S. Machado, Wolfram Ratzinger, Pedro Schwaller, and Ben A. Stefanek. Gravitational wave probes of axionlike particles. *Phys. Rev. D*, 102(7):075033, 2020.
- [33] Eric Madge, Wolfram Ratzinger, Daniel Schmitt, and Pedro Schwaller. Audible axions with a booster: Stochastic gravitational waves from rotating ALPs. *SciPost Phys.*, 12(5):171, 2022.
- [34] Jens Chluba, Liang Dai, Daniel Grin, Mustafa Amin, and Marc Kamionkowski. Spectral distortions from the dissipation of tensor perturbations. *Mon. Not. Roy. Astron. Soc.*, 446:2871–2886, 2015.
- [35] Athul K. Soman, Swagat S. Mishra, Mohammed Shafi, and Soumen Basak. Inflationary Gravitational Waves as a probe of the unknown post-inflationary primordial Universe. 7 2024.
- [36] Ken’ichi Saikawa and Satoshi Shirai. Primordial gravitational waves, precisely: The role of thermodynamics in the Standard Model. *JCAP*, 05:035, 2018.
- [37] Laurence F Abbott and Mark B Wise. Constraints on generalized inflationary cosmologies. *Nuclear physics B*, 244(2):541–548, 1984.
- [38] Varun Sahni. Energy density of relic gravity waves from inflation. *Physical Review D*, 42(2):453, 1990.
- [39] Rouzbeh Allahverdi et al. The First Three Seconds: a Review of Possible Expansion Histories of the Early Universe. 6 2020.
- [40] Nicolás Bernal and Fazlollah Hajkarim. Primordial Gravitational Waves in Nonstandard Cosmologies. *Phys. Rev. D*, 100(6):063502, 2019.
- [41] Daniel Grin, Tristan L. Smith, and Marc Kamionkowski. Axion constraints in non-standard thermal histories. *Phys. Rev. D*, 77:085020, 2008.
- [42] Gian F. Giudice, Edward W. Kolb, Antonio Riotto, Dmitry V. Semikoz, and Igor I. Tkachev. Standard model neutrinos as warm dark matter. *Phys. Rev. D*, 64:043512, 2001.
- [43] Gian Francesco Giudice, Edward W. Kolb, and Antonio Riotto. Largest temperature of the radiation era and its cosmological implications. *Phys. Rev. D*, 64:023508, 2001.
- [44] Daniel J. H. Chung, Edward W. Kolb, and Antonio Riotto. Production of massive particles during reheating. *Phys. Rev. D*, 60:063504, 1999.
- [45] M. Kawasaki, Kazunori Kohri, and Naoshi Sugiyama. MeV scale reheating temperature and thermalization of neutrino background. *Phys. Rev. D*, 62:023506, 2000.
- [46] Steen Hannestad. What is the lowest possible reheating temperature? *Phys. Rev. D*, 70:043506, 2004.
- [47] Francesco De Bernardis, Luca Pagano, and Alessandro Melchiorri. New constraints on the reheating temperature of the universe after WMAP-5. *Astropart. Phys.*, 30:192–195, 2008.
- [48] P. F. de Salas, M. Lattanzi, G. Mangano, G. Miele, S. Pastor, and O. Pisanti. Bounds on very low reheating scenarios after Planck. *Phys. Rev. D*, 92(12):123534, 2015.
- [49] Yann Gouttenoire, Geraldine Servant, and Peera Simakachorn. Kination cosmology from scalar fields and gravitational-wave signatures. 11 2021.
- [50] Sergey Alekhin et al. A facility to Search for Hidden Particles at the CERN SPS: the SHiP physics case. *Rept. Prog. Phys.*, 79(12):124201, 2016.
- [51] J. Beacham et al. Physics Beyond Colliders at CERN: Beyond the Standard Model Working Group Report. *J. Phys. G*, 47(1):010501, 2020.
- [52] Oleksii Mikulenko, Kyrylo Bondarenko, Alexey Boyarsky, and Oleg Ruchayskiy. New physics at the Intensity Frontier: how much can we learn and how? 12 2023.
- [53] Oleksii Mikulenko, Kyrylo Bondarenko, Alexey Boyarsky, and Oleg Ruchayskiy. Unveiling new physics with discoveries at Intensity Frontier. 12 2023.
- [54] Paul Frederik Depta, Marco Hufnagel, and Kai Schmidt-Hoberg. Robust cosmological constraints on axion-like particles. *JCAP*, 05:009, 2020.
- [55] Alexey Boyarsky, Maksym Ovchinnikov, Oleg Ruchayskiy, and Vsevolod Syvolap. Improved big bang nucleosynthesis constraints on heavy neutral leptons. *Phys. Rev. D*, 104(2):023517, 2021.
- [56] Jens Chluba and Donghui Jeong. Teasing bits of information out of the CMB energy spectrum. *Mon. Not. Roy. Astron. Soc.*, 438(3):2065–2082, 2014.
- [57] Ciaran O’Hare. cajohare/axionlimits: Axionlimits. <https://cajohare.github.io/AxionLimits/>, July 2020.
- [58] Peter Minkowski. $\mu \rightarrow e\gamma$ at a Rate of One Out of 10^9 Muon Decays? *Phys. Lett. B*, 67:421–428, 1977.

- [59] Rabindra N. Mohapatra and Goran Senjanovic. Neutrino Mass and Spontaneous Parity Nonconservation. *Phys. Rev. Lett.*, 44:912, 1980.
- [60] Rabindra N. Mohapatra and Goran Senjanovic. Neutrino Masses and Mixings in Gauge Models with Spontaneous Parity Violation. *Phys. Rev. D*, 23:165, 1981.
- [61] J. Schechter and J. W. F. Valle. Neutrino Masses in SU(2) x U(1) Theories. *Phys. Rev. D*, 22:2227, 1980.
- [62] M. Fukugita and T. Yanagida. Baryogenesis Without Grand Unification. *Phys. Lett. B*, 174:45–47, 1986.
- [63] Takehiko Asaka and Mikhail Shaposhnikov. The ν MSM, dark matter and baryon asymmetry of the universe. *Phys. Lett. B*, 620:17–26, 2005.
- [64] Sacha Davidson, Enrico Nardi, and Yosef Nir. Leptogenesis. *Phys. Rept.*, 466:105–177, 2008.
- [65] Kyrylo Bondarenko, Alexey Boyarsky, Juraj Klaric, Oleksii Mikulenko, Oleg Ruchayskiy, Vsevolod Syvolap, and Inar Timiryasov. An allowed window for heavy neutral leptons below the kaon mass. *JHEP*, 07:193, 2021.
- [66] Asli M. Abdullahi et al. The present and future status of heavy neutral leptons. *J. Phys. G*, 50(2):020501, 2023.
- [67] C. Ahdida et al. Post-LS3 Experimental Options in ECN3. 10 2023.
- [68] A. Blondel et al. Searches for long-lived particles at the future FCC-ee. *Front. in Phys.*, 10:967881, 2022.
- [69] M. Anelli et al. A facility to Search for Hidden Particles (SHiP) at the CERN SPS. 4 2015.
- [70] C. Ahdida et al. Sensitivity of the SHiP experiment to Heavy Neutral Leptons. *JHEP*, 04:077, 2019.
- [71] Stefan Antusch, Eros Cazzato, and Oliver Fischer. Sterile neutrino searches at future e^-e^+ , pp , and e^-p colliders. *Int. J. Mod. Phys. A*, 32(14):1750078, 2017.
- [72] Marcin Chrzaszcz, Marco Drewes, and Jan Hajer. HECATE: A long-lived particle detector concept for the FCC-ee or CEPC. *Eur. Phys. J. C*, 81(6):546, 2021.
- [73] Nashwan Sabti, Andrii Magalich, and Anastasiia Filimonova. An Extended Analysis of Heavy Neutral Leptons during Big Bang Nucleosynthesis. *JCAP*, 11:056, 2020.
- [74] Wolfram Ratzinger, Pedro Schwaller, and Ben A. Stefanek. Gravitational Waves from an Axion-Dark Photon System: A Lattice Study. *SciPost Phys.*, 11:001, 2021.
- [75] Enrico Morgante, Wolfram Ratzinger, Ryosuke Sato, and Ben A. Stefanek. Axion fragmentation on the lattice. *JHEP*, 12:037, 2021.
- [76] Raymond T. Co and Keisuke Harigaya. Axiogenesis. *Phys. Rev. Lett.*, 124(11):111602, 2020.
- [77] Raymond T. Co, David Dunsky, Nicolas Fernandez, Akshay Ghalsasi, Lawrence J. Hall, Keisuke Harigaya, and Jessie Shelton. Gravitational wave and CMB probes of axion kination. *JHEP*, 09:116, 2022.
- [78] George Hobbs and Shi Dai. Gravitational wave research using pulsar timing arrays. *National Science Review*, 4(5):707–717, 12 2017.
- [79] Andrea N. Lommen. Pulsar timing arrays: the promise of gravitational wave detection. *Rept. Prog. Phys.*, 78(12):124901, 2015.
- [80] Daniel J. Reardon et al. Search for an Isotropic Gravitational-wave Background with the Parkes Pulsar Timing Array. *Astrophys. J. Lett.*, 951(1):L6, 2023.
- [81] Craig Cahillane and Georgia Mansell. Review of the Advanced LIGO Gravitational Wave Observatories Leading to Observing Run Four. *Galaxies*, 10(1):36, 2022.
- [82] Michele Maggiore et al. Science Case for the Einstein Telescope. *JCAP*, 03:050, 2020.
- [83] Jeff Crowder and Neil J. Cornish. Beyond LISA: Exploring future gravitational wave missions. *Phys. Rev. D*, 72:083005, 2005.
- [84] Nancy Aggarwal et al. Challenges and opportunities of gravitational-wave searches at MHz to GHz frequencies. *Living Rev. Rel.*, 24(1):4, 2021.